Available online at www.derpharmachemica.com

ISSN 0975-413X
CODEN (USA): PCHHAX

Der Pharma Chemica, 2016, 8(4):67-76
(http://derpharmachemica.com/archive.html)

New class of Copper (II) complex derived from Isatin and Thiosemicarbazide - Synthesis, Spectral Characterization and biological activity

P. S. Suja Pon Mini[1], S. Theodore David Manickam[1*], R. Antony[2], S. Muthupoongodi[1] and S. Magala Sathyasheeli[3]

[1]Centre for Scientific and Applied Research (C-SAR), PSN College of Engineering and Technology, Tirunelveli, 627 152, Tamil Nadu, India
[2]Department of Chemistry, Indian Institute of Technology Bombay, Mumbai-400076, India
[1]Infant Jesus college of Engineering, Keelavallanadu, Thoothukudi, India

---

ABSTRACT

A new class of Schiff base derived from Isatin and Thiosemicarbazide (AB) and its Cu(II) complex were synthesized and characterized by elemental analysis, magnetic study, molar conductance measurement and spectroscopic methods viz.[13]CNMR, FT-IR, UV, CV, ESR, XRD and Fluorescence spectra as well as thermal studies. The Schiff base coordinates the Copper (II) ion in a tetradentate manner. The elemental analysis suggests the stoichiometry to be 1:1 (metal: ligand). The cyclic voltammogram of the Copper (II) complex in DMSO solution exhibit metal centered electro activity in the potential range -1.0 to 1.0V with scan rate 10 mV/s. The g values calculated for Copper(II) complex indicate the presence of the unpaired electron in the d_{x2-y2} orbital. A further XRD study reveals the crystalline nature of both the ligand and the Cu(II) complex. The ligand and the Copper(II) complex have been found to exhibit effective antimicrobial activity tested against selected gram positive and gram negative bacterial as well as fungal species.

Key words: Isatin, Thiosemicarbazide, ESR, Corrosion, DNA binding.

INTRODUCTION

Schiff bases and its metal complexes have been widely investigated, due to their incredible chemical properties and applications in various areas [1-3]. Thiosemicarbazide and its derivatives as ligands with potential sulphur and nitrogen are fascinating and have achieved unique attention due to their importance in therapeutic and pharmaceutical field. They show biological activities consisting of antibacterial, antifungal, anticancer, herbicidal, anticorrosion and anti-inflammatory activities [4-6]. Isatin based Schiff bases are also chemically more potent due to their versatility [7-8]. Keeping these in mind, herein we report the synthesis, structural characterisation, antimicrobial, anticorrosion and DNA binding study of the Schiff base derived from isatin and thiosemicarbazide and its Copper (II) complex.

MATERIALS AND METHODS

2.1. Reagents and instrumentation

The chemicals Isatin, thiosemicarbazide, Copper (II) Chloride and the solvents used were of analytical grade and purchased from High media. A CARLO ERBA 1108 elemental analyzer was employed to obtain the micro analytical data (C, H & N) of the compounds using sulphanilamide as the reference standard. The Cu(II) was estimated using standard experimental methods [9]. FTIR spectra (4000-400 cm-1) were recorded with KBr pellets on Jasco FTIR/4100 spectrophotometer annexed with ATR accessory at a resolution of $4cm^{-1}$. Electronic spectrum was recorded on a Shimadzu UV-1601 spectrophotometer in the wave length region of 200-800 nm. ^{13}CNMR spectra were recorded on a Bruker DRX-500 MHz, AVANCE spectrometer at ambient temperature in DMSO-*d*6 using TMS as internal standard. Cyclic Voltammetric studies were carried out at room temperature with a BAS CV-27 Electrochemical analyzer in DMSO solution containing 0.1M $NaClO_4$ using a glassy carbon electrode. A platinum wire and saturated Hg_2Cl_2 were used as counter and reference electrodes respectively. Molar conductivity measurements were recorded on a Deep vision model 601 digital conductivity meter. For magnetic susceptibility measurements were recorded by Guoy balance at room temperature, using $CuSO_45H_2O$ as the calibrant. The EPR measurements were performed on a JEOL JES TE300 spectrometer. XRD determinations were made using an X-ray diffractometer (XPERT PRO PANalytical).Thermo gravimetric (TG) studies were manipulated under a dynamic N_2 atmosphere in the 20-800 °C temperature range at a heating rate of $10\,^{\circ}C\ min^{-1}$ on a Mettler Toledo star system. The fluorescence studies of Schiff base and its metal complex were recorded on HITACHI F-7000 fluorescence spectrophotometer.

2.2. Synthesis of ligand and Copper (II) complex

2.2.1. Synthesis of isatin based Schiff base L

2 mmol of methanolic solution of isatin (A) was stirred for 2 h in a 50 ml flask using a magnetic stirrer. To the resulting methanolic suspension of isatin, 2mmol of thiosemicarbazide (B) was added .The mixture was allowed to react in another flask equipped with the magnetic stirrer for 24h .The obtained product, Schiff base AB, was filtered, washed with methanol followed by ether and dried at 70 °C in vacuum.

2.2.2. Synthesis of Copper (II) complex

1 mmol of the purified AB was added to 1 mmol methanolic solution of $CuCl_2$ and refluxed for 8 h. The resultant product, CuAB, was filtered and washed well with ether and dried at 70 °C in vacuum.

2.3. Biological activity

2.3.1. Antimicrobial activity (invitro)

The synthesized Schiff base (AB) and the CuAB complex were tested against the gram positive, negative bacterial species and fungal species *pseudomonas aeruginosa* and staphylo *coccus* as well as fungi *aspergillus niger,* by agar diffusion method. Initially the stock cultures of bacteria were revived by inoculating in brothmedia and grown at 37 ° C for 18 hours. The agar plates of the media were prepared and the wells were made in the plate. With 18 hour old cultures each plate was inoculated and spread over the plates. The required concentration of the test sample was introduced into the respective wells. The control wells with gentamycin were also prepared. DMSO was used as negative control. The plates were incubated at 37 ° C for 20 hours. Activity was determined by measuring the diameter of zones showing complete inhibition.

2.3.2 DNA binding experiments

The interaction between metal complexes and DNA was studied using electronic absorption methods. Disodium salt of calf thymus DNA was stored at 4˚C. Solution of DNA in the buffer 50 mM NaCl/ 5 mM Tris–HCl (pH 7.2) in water gave a ratio 1.9 of UV absorbance at 260 and 280 nm, A260/A280, indicating that the DNA was sufficiently free from protein . The concentration of DNA was measured using its extinction coefficient at 260 nm (6600M_1 cm_1) after 1:100 dilutions. Stock solutions were stored at 4˚C and used for not more than 4 days. Doubly distilled water was used to prepare solutions. Concentrated stock solutions of the complexes were prepared by dissolving the complexes in DMSO and diluting suitably with the corresponding buffer to the required concentration for all of the experiments.

RESULTS AND DISCUSSION

3.1. Micro Analysis and Molar Conductance measurements

The molar conductivity of the Copper (II) complex (CuAB) at room temperature was measured in DMSO. The conductance data, shown in Table 1, indicate that CuAB is non ionic in nature. The micro analysis results of the synthesized Schiff base complex CuAB given in Table 1 suggest that Schiff base ligand is potentially tetradentate and form complex in 1:1 ratio metal to ligand. The proposed structure is given in Figure 1.

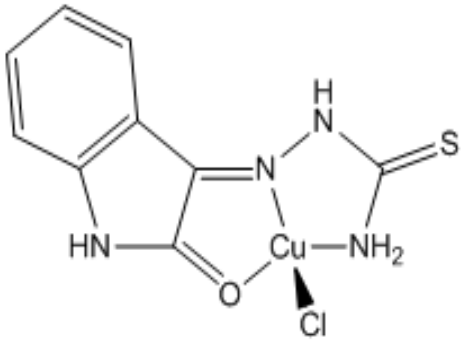

Figure 1 Structure of CuAB

Table 1 Physical and Analytical Data of CuAB

Molecular Formula	Molecular Weight	Molar Conductance (S cm^2 mol^{-1})	Magnetic moment B.M.	Colour	Elemental analysis (Theoretical values in parenthesis)		
					C	H	N
$C_9H_8N_4OS$ CuCl	319.25	17.86	1.6	Dark Yellow	33.05 (33.86)	2.58 (2.53)	17.97 (17.55)

3.2 ^{13}CNMR Spectral Studies

The ^{13}CNMR spectra of the Schiff base AB (Figure 2), confirms the presence of various types carbons of the compound which are chemically non-equivalent. The signals at 120.023 ppm, 121.771 ppm 123.856 ppm, 143.437 ppm, and 152.345 ppm are due to carbons of isatin moiety. A characteristic signal for the imino carbon (C=N) appears at 163.237 ppm authenticates the formation of Schiff base. In addition, the signals obtained in the region 79.865 ppm, 111.236 ppm, 119.458 ppm are assigned to aromatic carbon [10].

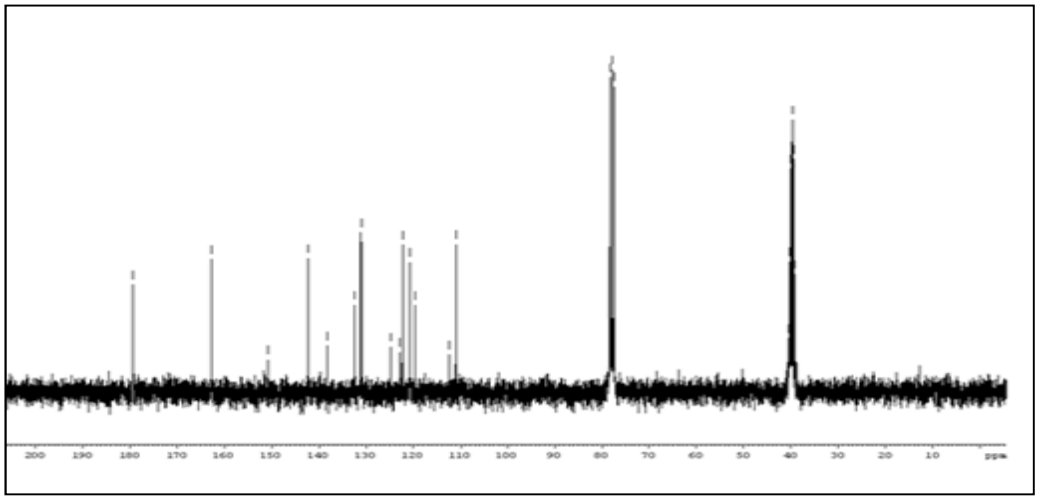

Figure 2 ^{13}CNMR of the ligand AB

3.3 Vibrational Spectral Studies

The FT-IR spectrum of the ligand AB, and CuAB are given in Figure 3 and 3a. AB shows a broad band in the range of 3250-3500 cm^{-1} assigned to the stretching vibrations of NH_2 group of thiosemicarbazide. The bands observed at 1590 cm^{-1}, 1700 cm^{-1} and 1100 cm^{-1} can be attributed to N-H stretching, –C=O stretching and -C=S stretching of thiosemicarbazide moiety. The strong band observed at 1671 cm^{-1} could be assigned to -C=N stretch which further confirms the formation of Schiff base from thiosemicarbazide and isatin. In CuAB, the imino stretching frequency appears at 1591 cm^{-1}, compared to 1671 cm^{-1} of the free ligand AB. This shift to the lower frequency region clearly indicates the coordination of the imino nitrogen atom to the Cu (II) ion. Also the absorption peak due to N-H stretching of thiosemicarbazide has been shifted from 1590 cm^{-1} to 1500 cm^{-1}, which clearly reveal the coordination of amino group (present in thiosemicarbazide) to the Cu(II) ion. Furthermore, the absorption peak due to the amido group (present in isatin moiety), has been shifted from 1700 cm^{-1} to 1698 cm^{-1}, which clearly shows its coordination with the central Cu(II) ion. Further, the appearance of new bands at 583 cm^{-1}, 490 $cm^{-1}$and 449 cm^{-1} clearly evidences the formation of Cu-N, Cu-O and Cu-Cl bonds respectively [10,13].

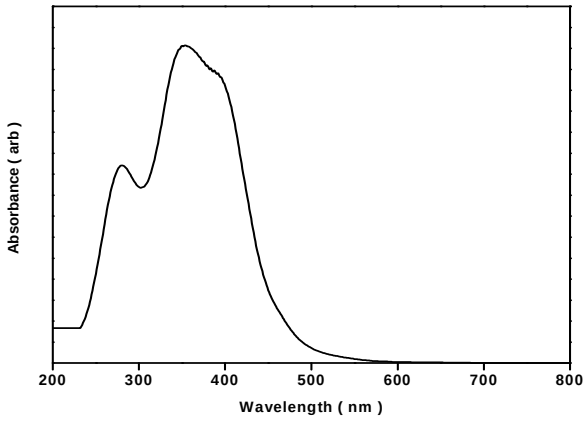

Figure 3 FT-IR Spectrum of AB

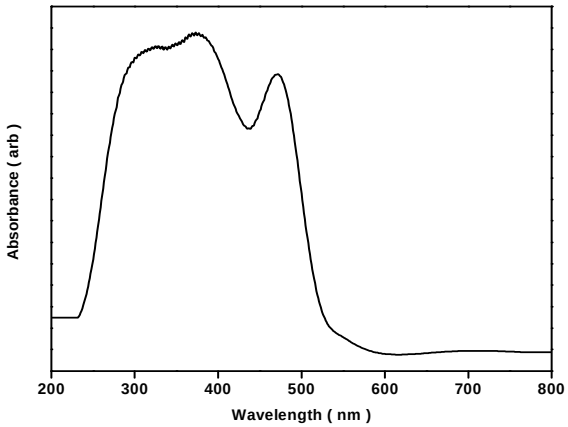

Figure 3a FT-IR Spectrum of CuAB

3.4 Electronic Spectral Studies

The UV spectrum of AB and CuAB are portrayed in Figure 4 and 4a. The ligand AB shows significant absorption bands at 290 nm & 340 nm may be attributed to the π-π* transitions of -C=C, -C=N and -C=O groups and n-π* transitions of –C=N and –C=O groups, present in AB. CuAB also exhibits characteristic bands of π-π*and n-π* at 300 and 400 nm, respectively .In addition to this another band centered at around 480 nm is obtained, which can be attributed to $^2B_{1g} \rightarrow {}^2A_{1g}$ d-d transition arising due to dsp^2 hybridization, leading to square planar geometry around copper(II). This also validates the coordination of Cu(II) metal ion with ligand AB [11,12].

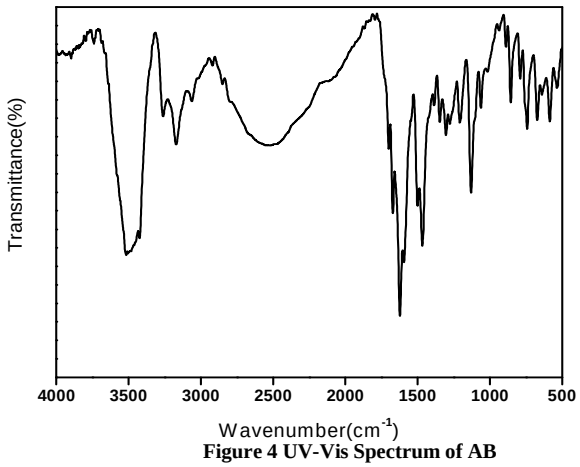

Figure 4 UV-Vis Spectrum of AB

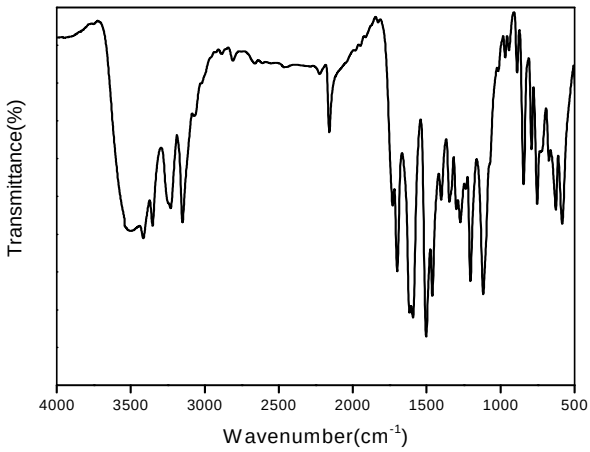

Figure 4a UV-Vis Spectrum of CuAB

3.5 Thermal Studies

The TG-DTG pattern of AB and CuAB are portrayed in Figure 5 and 5a. The Schiff base ligand AB shows three mass loss stages. They are 50-110°C (5%), 150 -280°C (21%) and 280-470°C (27%). The first stage is due to the loss of water molecules and methanol molecules from the ligand. The second and third stages may be attributed to the decomposition of thiosemicarbazide group and the isatin moiety respectively. In CuAB, also three mass loss stages are noticed and they are 50-210°C (19%), 250-360°C (18%) and 360-460°C (15%). The first stage is due to the loss of water molecules, methanol molecules and chlorine atom from the complex. The second and third stages may be attributed to the decomposition of Thiosemicarbazide group and the isatin moiety. The remaining materials are the residual metal oxide obtained above 700°C. According to the DTG curves of AB & CuAB all the thermal decays involved endothermic decomposition [14, 15].

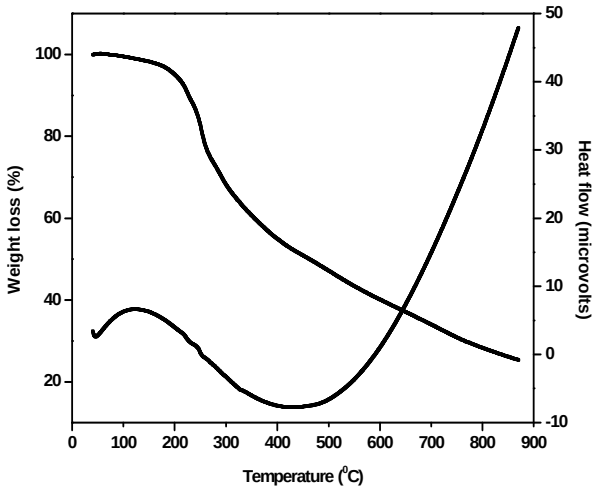

Figure 5 TG/DTG pattern of AB

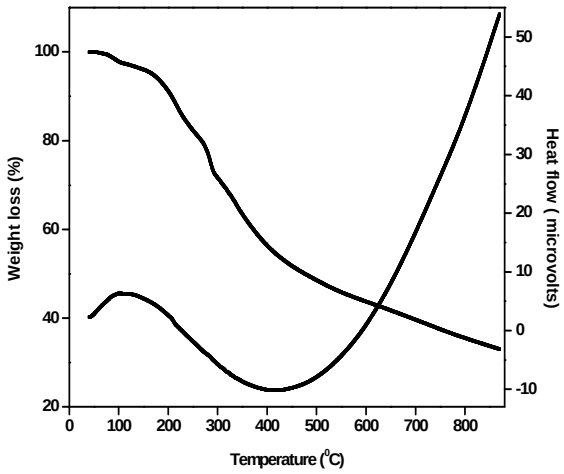

Figure 5a TG/DTG pattern of CuAB

3.6 Emission Spectral Studies

The emission spectrum of the Schiff base ligand AB and CuAB have been depicted in Figure 6 and 6a. When excited at 300 nm, the ligand AB fluoresced at 436 nm in visible region, assigned to the intraligand fluorescent emission which is related to the energy gap between the $\pi \rightarrow \pi^*$ molecular orbital of the π–conjugation of the ligand system attributed to the large dipole moment of the fluorescent excited state and the hydrogen bonds formed between AB and the solvent. Moreover it has been suggested that the fluorescence of AB is probably quenched by the appearance of photo induced electron transfer (PET) process due to the presence of lone pair of electrons on the nitrogen atom of AB. CuAB complex exhibits the emission band at around 440 nm with higher fluorescent intensity upon excitation at 315 nm. It may be ascribed to intraligand transition mixed with metal - ligand charge transfer (M-LCT) and are slightly red shifted when compared to that of the ligand. Moreover it has been observed that coordination of Cu(II) ion with the ligand can quench the fluorescence emission [17-18].

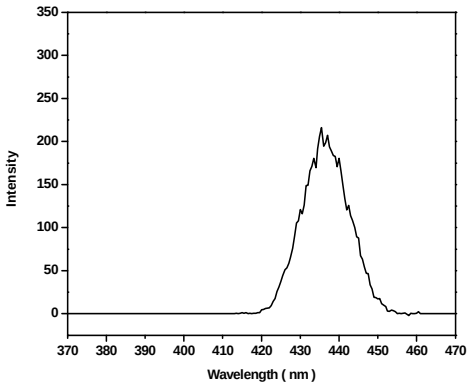

Figure 6 Emission Spectrum of AB

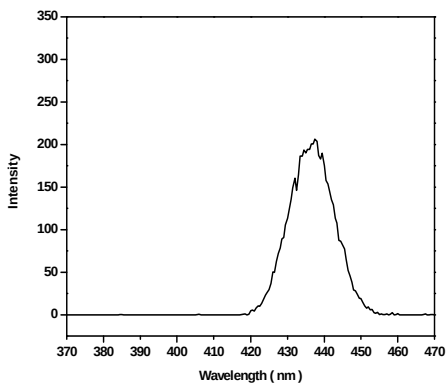

Figure 6a Emission Spectrum of CuAB

3.7 Powder XRD Analysis

The XRD pattern of AB and CuAB are shown in Figure 7 and 7a. AB shows its characteristic peak at 2θ = 12.8410 with d spacing 6.89418. It indicates the crystalline nature of the ligand. The powder XRD of CuAB measured between 2θ ranging from 8° to 32° with maxima at 2θ = 15.7442 corresponds to the inter-planar distance = 6.89418. Both the powder XRD pattern of the AB and CuAB are very similar with each other. This clearly demonstrates that the crystallinity of AB have not been altered even after the complexation of Cu(II). It is further confirmed by calculating the grain size of AB and CuAB using Scherrer's formula $d_{xrd} = 0.9\lambda / \beta\cos\theta$, where d_{xrd} is the particle size, λ is the wavelength of the radiation, β is the full – width half maximum and θ is the diffraction angle for hkl plane. Both AB and CuAB are nanocrystalline with grain size in the range 24 to 25 [14].

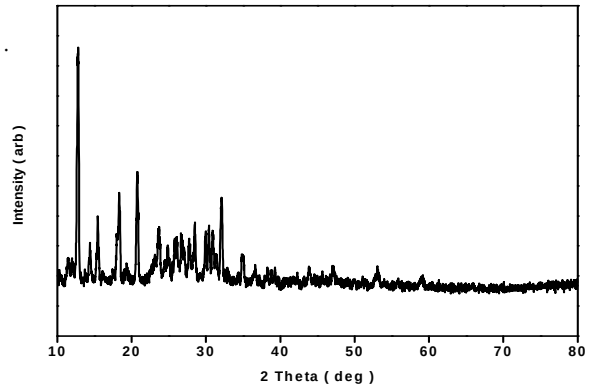

Figure 7 Powder XRD pattern of AB

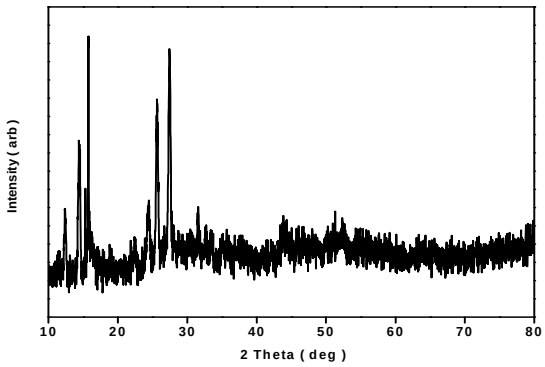

Figure 7a XRD pattern of CuAB

3.8 Electrochemical Studies

The cyclic voltammogram of CuAB is illustrated in Figure 8. It shows a significant electrochemical process, which is found to follow the one electron reversible mechanism. This reversible process includes the cathodic peak at 0.31 V (Epc) which corresponds to the reduction of Cu(II) to Cu(I) and the anodic peak at -0.30 V (Epa) which is a characteristic of the reversible oxidation of Cu(I) to Cu(II). The reversible nature of this process is confirmed by the calculated current ratio value (ipc/ipa), which is equal to 1[13].

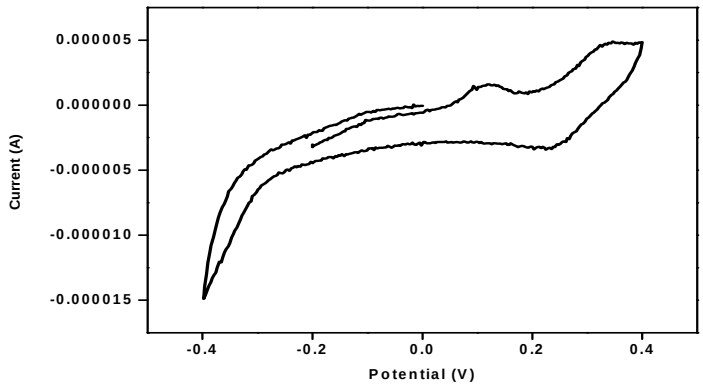

Figure 8 Cyclic Voltammogram of CuAB

3.9 ESR Spectroscopy

The ESR spectrum of the CuAB complex recorded in DMSO at room temperature is shown in the Figure 9. It has been observed that the $g_{\parallel}$ value is 2.25 and the $g_{\perp}$ value is 2.1. The trend $g_{\parallel} > g_{\perp} > 2.0023$ indicated that the unpaired electron is localized in the dx^2-y^2 of the Cu(II) ion and is characteristic of the square planar geometry. The g_{ave} was found to be 2.17 .The deviation of g_{ave} from that of the free electron is due to the covalent character. Finally G is calculated by using the expression $G = g_{\parallel} -2/g_{\perp}-2$. The G value of 2.5 indicates negligible exchange interaction between metal centres's in solid complex. Therefore ESR studies validates that the complex CuAB exhibits square planar geometry [16, 19].

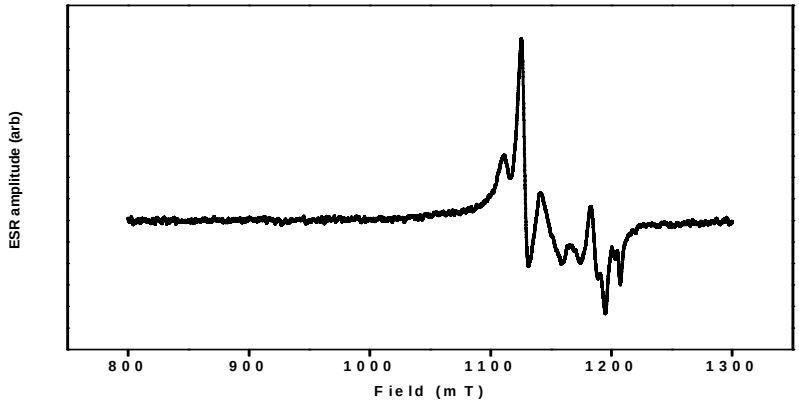

Figure 9 ESR Spectrum of CuAB

3.10 Corrosion studies

Corrosion inhibition is ascribed to the adsorption of inhibitor on aluminium foil. The graphical presentation of variation of the inhibitor efficiency with concentration of AB is given in Figure 10 and that of surface coverage in Figure 10a. The results (Table 2) indicate that the inhibition efficiency increases with the concentration of the inhibitor. The lone pair of electrons on N and O atoms along with the delocalized pi electrons can be the reason for high inhibition efficiency. As inhibitor concentration increases, it covers more and more surface area and results in the reduction of corrosion rate. The results indicate that the inhibition efficiency increases with the concentration of the inhibitor. It increases steadily as the concentration increases. The maximum efficiency of 71.1 % was observed for 1 mmol concentration of AB. The surface coverage of the inhibitor increases slowly and steadily with the increase in concentration. Further the inhibition efficiency of AB can be evidenced by taking the optical image and is shown in Figure 11. The corrosion tendency has been reduced in a very good manner with inhibitor AB due to the lone pair electrons of nitrogen and oxygen atoms along with the delocalized π-electrons. It can be explained on the basis of the effect of chemical structure. In this respect the isatin ring, N-H, C=O, C=N and C=S of thiosemicarbazide can form a big π bond. These bonds produce more than one centre of chemical adsorption on aluminium foil thus preventing corrosion [20].

Table 2 Corrosion inhibition efficiency & surface coverage of aluminium sheet by AB

S.No	Conc.(m mol)	Weight loss (g)	Inhibition Efficiency (%)	Surface Coverage (θ)	log C	log (θ/1- θ)
1	Blank	0.00045	-	-	-	-
2	0.2	0.00036	20.00	0.20	-0.6989	-0.6020
3	0.4	0.00027	40.00	0.40	-0.3979	-0.1760
4	0.6	0.00020	55.56	0.56	-0.2218	0.0969
5	0.8	0.00018	60.00	0.60	-0.0969	0.1760
6	1	0.00013	71.11	0.71	0	0.3912

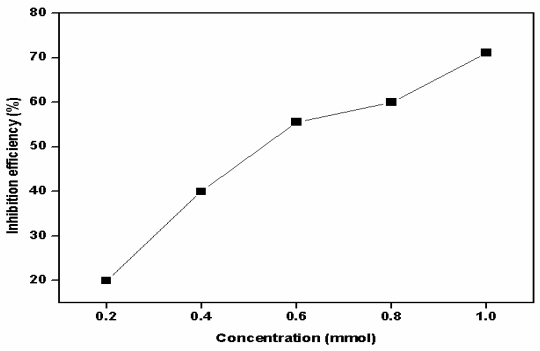

Figure 10 Corrosion inhibition efficiency of AB

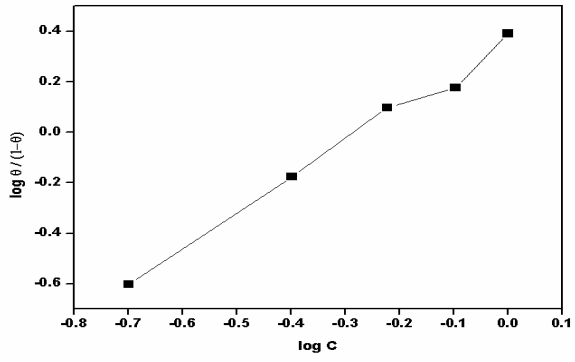

Figure 10a Surface coverage of AB

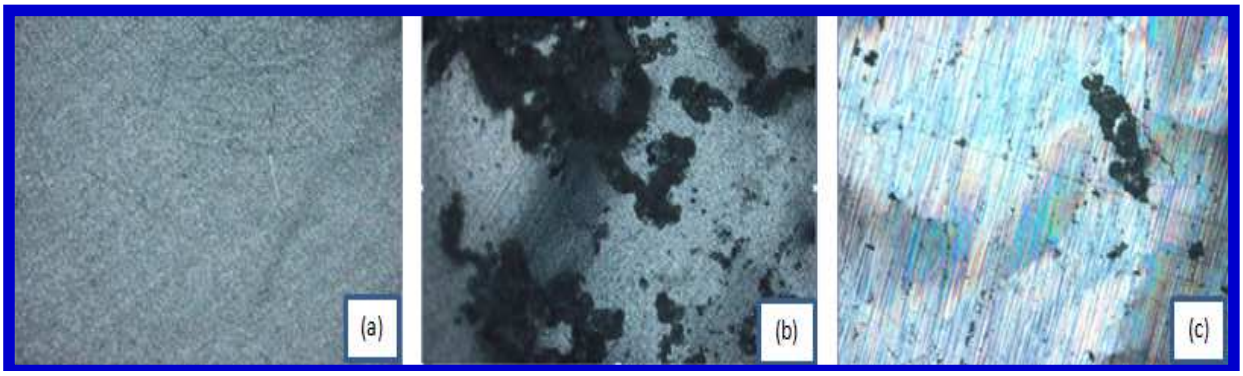

Figure 11(a) Optical image of aluminium sheet (b) acid treated aluminium sheet without inhibitor (c) acid treated aluminium sheet with inhibitor AB

3.11 DNA binding studies of CuAB (Absorption)

The electronic absorption titration of CuAB has been carried out at a fixed concentration of the complex in DMSO at 25^{o}C, varying the concentration of DNA and is illustrated in Figure 12. The absorption spectra of CuAB show band in the region 300 nm and is assigned to ligand to metal charge transfer (LMCT) transitions. When the amount of DNA is increased, the intensity of the charge transfer band is also changed, due to either hypochromism or hyperchromism. The complex CuAB shows hypochromism with very slight red shift in the presence of DNA characteristic of intercalation which is attributed to the interaction between the aromatic chromophore ligand of metal complex and the base pairs of DNA. When the ligand of isatin based Copper (II) complex intercalated into the base pairs of DNA, its π^* orbital was coupled with the π orbital of DNA base pairs to give rise to the decrease in the π-π^* transition energies. As a result the λ_{max} of the intra ligand transition of the ligand was shifted to the longer wavelength (red shift) [21].

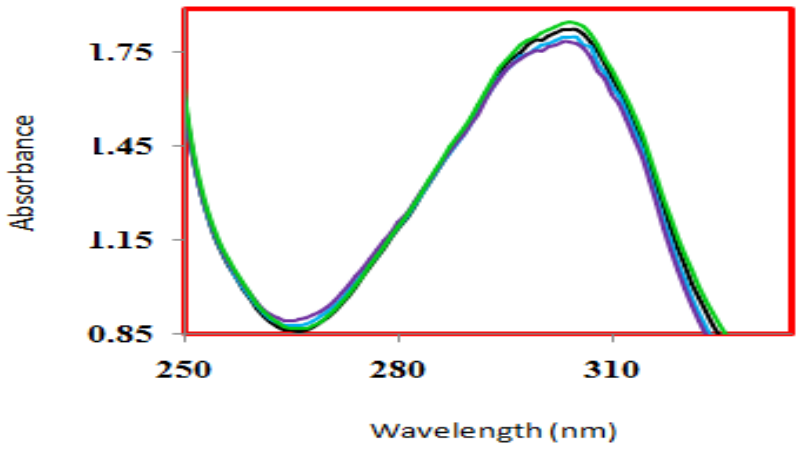

Figure 12 Absorption spectra of CuAB in presence of DNA

3.12 Antimicrobial studies

A comparative study of the growth inhibition zone values of AB and CuAB are shown in Table 3. Figure 13 show that both the ligand AB and CuAB exhibit better antimicrobial activity. The antimicrobial activity depends upon the following components.

- The chelating ability of the ligand
- The nature of nitrogen donor ligand
- The total charge of the complex
- The existence and nature of the metal ion

The enhancement in the activity can be due to the azomethine linkage (C=N) in their structure. It has been suggested that the enzyme production might be reduced with nitrogen and oxygen donor systems, because they are more susceptible to deactivation by the metal ion upon chelation. The polarity of the metal ion is reduced by chelation and it is due to the partial sharing of its positive charge with the donor groups and the delocalized π electrons within the whole chelation ring which is formed because of the coordination [21].

Table 3 Antimicrobial activity of Schiff base AB & CuAB by disc diffusion method (Zone formation in mm)

Ligand/Complex	Pseudomonas (mm)	Staphylo coccus (mm)	Aspergillus (mm)
AB	9	9	6
CuAB	8	7	7

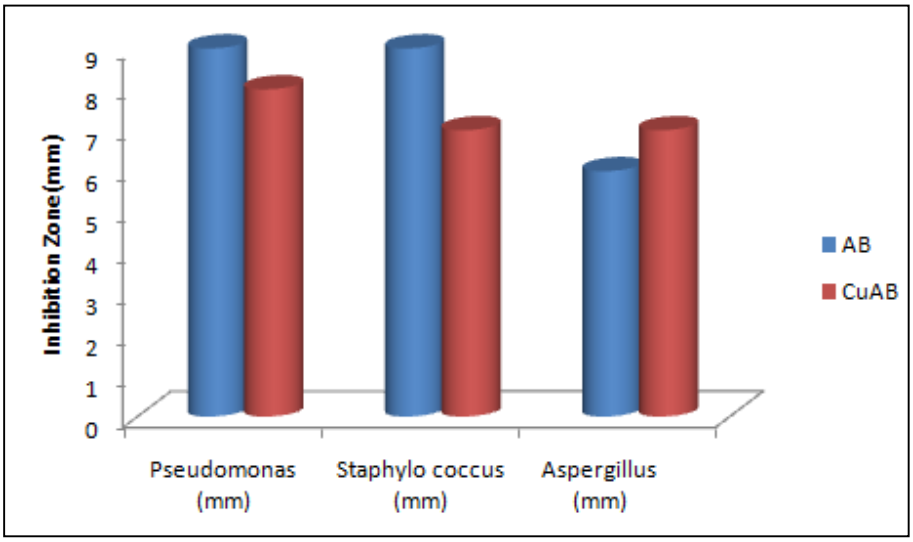

Figure 13 Antimicrobial activity of Schiff base AB & CuAB by disc diffusion method (Zone formation in mm)

CONCLUSION

A new class of Schiff base ligand (AB) has been synthesized from isatin and thiosemicarbazide by condensation. Its Copper (II) complex has also been synthesized and characterized by various spectro analytical data. Schiff base ligand AB coordinate the Cu(II) ion through the imino nitrogen atom, one amino nitrogen atom of thiosemicarbazide moiety, the amido oxygen atom of isatin moiety and one chlorine atom. Hence square planar geometry was assigned to CuAB by electronic spectral evidences which were also supported by EPR spectra. The XRD studies clearly reveal that both the Schiff base ligand and the CuAB complex are nanocrystalline. The TG/DTG analysis indicates that both the ligand and the CuAB are thermally stable. The antimicrobial studies reveal that the ligand and CuAB show greater activity. The corrosion inhibition studies clearly indicate that the ligand AB act as a very good corrosion inhibitor. The DNA electronic absorption studies of CuAB show hypochromism with slight red shift in the presence of DNA characteristic of intercalation between the aromatic chromophore ligand of metal complex and the base pairs of DNA.

REFERENCES

[1] T P Yoon and E N Jacobsen, “Privileged Chiral Catalysts”, *Science*, **2003**, 299, 1691.
[2] M G Juan Fernandez, A Fred, Lopez-DURAN, Simon Hernandez-Ortega, Virginia Gomez-Vidales, Norma Macias- Ruvalcaba, Martha Aguilar-Martinez, *Journal of Molecular structure* **2002**, 612, 69-79
[3] A A Khandar, K Nejati, *Polyhedron*, **2000**, 19, 607-613
[4] Mustafa Dolaz, Vickie Mckee, Serhan Urus,Necmettin Demir, Ali Sabik, Aysegul, Golcu, Mehmet Tumer, *Spectrochimica Acta Part A* **2010**, 76, 174-181
[5] Chandan Adhikary, Rajesh Bera, *Polyhedron*, **2008**, 27, 1556-1562
[6] Esin Ispir, *Dyes and Pigments*, **2009**, 82, 13-19

[7] C Joel, S Theodore David, R Biju Bennie, S Daniel Abraham, and S Iyyam Pillai, *Journal of Chemical and Pharmaceutical Research*, **2015**, 7, 1159-1176.
[8] C Joel, S Theodore David, R Biju Bennie, S Daniel Abraham, S Iyyam Pillai, and S Magala Sathyasheeli, *International Journal of Research in Inorganic Chemistry*, **2015**, 5, 14-20.
[9] S A Patil, S N Unki, A D Kulkarni,V H Naik & P S Badami, *Spectrochimica Acta Part A: Molecular and Biomolecular Spectroscopy*, **2011**, 79, 1128-1136.
[10] S A Patil, S N Unki, *Journal of Molecular Structure*, **2011**, 985, 330-338.
[11] A N Kursunlu, E Guler, F Sevgi & B Ozkalp, *Journal of Molecular Structure*, **2013**, 1048, 476-481.
[12] P S Suja Pon Mini, R Antony, S Theodore David Manickam, *Journal of New Materials for Electrochemical Systems*, **2014**, 17, 179-183.
[13] M Neelakantan, F Rusalraj, *Spectrochimica Acta Part A: Molecular and Biomolecular Spectroscopy*, **2008**, 71, 1599-1609.
[14] R Antony, S T David, K Saravanan, K Karuppasamy & S Balakumar, *Spectrochimica Acta Part A: Molecular and Biomolecular Spectroscopy*, **2013**, 103, 423-430.
[15] R Antony, S T D Manickam, K Saravanan, K Karuppasamy & S Balakumar, *Journal of Molecular Structure*, **2013**, 1050, 53-60.
[16] E Aazam, A E Husseiny, & H Al-Amri, *Arabian Journal of Chemistry*, **2012**, 5, 45-53.
[17] S Basak, S Sen, S Banerjee, S Mitra, G Rosair & M G Rodriguez, *Polyhedron*, **2007**, 26, 5104-5112.
[18] S A Patil, S N Unki, A D Kulkarni, V H Naik, U Kamble & P S Badami, *Journal of Coordination Chemistry*, **2011**, 64, 323-336
[19] R A Hameed, H Al-Shafey, *J. Mater. Environ. Sci*, **2012**, 3, 294.
[20] N Raman, R Jeyamurugan, R U Rani, T Baskaran & L Mitu, *Journal of Coordination Chemistry*, **2010**, 63, 1629-1644.
[21] N Raman, S Sobha & A Thamaraichelvan, *Spectrochimica Acta Part A: Molecular and Biomolecular Spectroscopy*, **2011**, 78, 888-898.